

Robust optimal density control of robotic swarms

Carlo Sinigaglia, Andrea Manzoni, Francesco Braghin, and Spring Berman

Abstract—In this paper, we propose a computationally efficient, robust density control strategy for the mean-field model of a robotic swarm. We formulate a static optimal control problem (OCP) that computes a robot velocity field which drives the swarm to a target equilibrium density, and we prove the stability of the controlled system in the presence of transient perturbations and uncertainties in the initial conditions. The density dynamics are described by a linear elliptic advection-diffusion equation in which the control enters bilinearly into the advection term. The well-posedness of the state problem is ensured by an integral constraint. We exploit the kernel properties of the state operator to show the uniqueness of the optimal solution and global asymptotic stability of the controlled system. The resulting control field is space-dependent and does not require any communication between robots or costly density estimation algorithms. Based on the properties of the primal and dual systems, we first propose a method to accommodate the state constraint. Exploiting the properties of the state dynamics and associated controls, we then construct a modified dynamic OCP to speed up the convergence to the target equilibrium density of the associated static problem. We then show that the finite-element discretization of the static and dynamic OCPs inherits the structure and several useful properties of their infinite-dimensional formulations. Finally, we demonstrate the effectiveness of our control approach through numerical simulations of scenarios with obstacles and an external velocity field.

Index Terms—Density Control, Optimal Control, Distributed Parameter Systems, Bilinear Control Systems, Finite Element Method, Mean-field Models

I. INTRODUCTION

LARGE-SCALE collectives of robots, or robotic swarms, are increasingly finding applications in a variety of tasks, such as search-and-rescue missions, infrastructure inspection and maintenance, precision agriculture, and many others [1]. This is in part due to the significant decrease in the cost of electronic components over the past few decades, which facilitates the fabrication of very large numbers of robots. Due to size and economic constraints, the computational power of a single swarm member is necessarily limited, which restricts the complexity of its control algorithms. From a control-theoretic point of view, the challenge is to synthesize controllers that can be implemented on swarms of such robots to produce collective behaviors that achieve specified high-level tasks, in a way that accommodates the high dimensionality of the system.

Submitted to IEEE Transactions on Automatic Control on May 26, 2022. This work was supported by the Italian Ministry of Education, University and Research (MIUR).

C. Sinigaglia and F. Braghin are with the Department of Mechanical Engineering, Politecnico di Milano, Milano, 20156 Italy (e-mail: carlo.sinigaglia@polimi.it; francesco.braghin@polimi.it).

A. Manzoni is with the MOX Department of Mathematics, Politecnico di Milano, Milano, 20133 Italy (e-mail: andrea1.manzoni@polimi.it)

S. Berman is with the School for Engineering of Matter, Transport and Energy, Arizona State University, Tempe, AZ 85287 USA (e-mail: spring.berman@asu.edu)

Classical path planning and control algorithms either do not scale well with the number of robots or do not allow the designer to specify complex high-level objectives. Recently, macroscopic descriptions of swarm dynamics in the form of mean-field models [2] have been used to devise robust path planning algorithms for robotic swarms to perform collective tasks such as coverage and mapping [3], [4]. Mean-field models provide a general probabilistic framework that can be used to design control algorithms for swarms of agents with stochastic behaviors. In this framework, swarm tasks are specified in terms of macroscopic population dynamics that are described by a mean-field model, and this model is used to derive the robot control policies, which guide the microscopic dynamics of individual robots and drive the swarm to collectively reproduce the macroscopic dynamics in expectation. A consistent way of analyzing the performance of such control policies when they are implemented on a finite number of robots has been developed in [5].

In the mean-field setting, the robotic swarm is represented by a probability density, which is independent of the number of robots, that evolves over space and time according to a Kolmogorov forward equation. Finite-dimensional mean-field models consist of a linear system of ordinary differential equations (ODEs) describing the dynamics of a swarm that evolves according to a Markov chain over a finite state space, which consists of a set of tasks or discrete spatial locations (e.g., [6]). One type of infinite-dimensional mean-field model is a linear parabolic advection-diffusion partial differential equation (PDE) governing the space-time dynamics of a swarm that follows a deterministic velocity field perturbed by noise, modeled by a Wiener process, over a continuous state space.

Recently developed control strategies for swarms based on mean-field models often rely on estimation of the local swarm density at each instant [7], [8], which is implemented with decentralized estimation algorithms that are computationally costly and require inter-robot communication. The work [8] synthesizes control laws that are inversely proportional to the estimated density, which generates unphysically high velocity fields when the density is small. On the other hand, Markov chain-based probabilistic algorithms for swarm density control, such as [9], do not necessarily require communication between robots and provide interesting self-healing properties. However, an *a priori* discretization of the state space is needed to set up the control problem in the Markov-chain framework. The control laws in [9] do not depend on the estimated swarm density, but rather are implicit functions of the target swarm density and the state-space discretization.

In this paper, we propose an optimization-based algorithm for computing a feedback control law that steers a swarm of agents with both advective and diffusive motion towards a target equilibrium density. The control law is defined as

the advection field and depends only on space, not on the estimated swarm density or the initial conditions of the swarm, and can be preprogrammed on simple agents without inter-agent communication. Our approach is similar to [9], but in contrast to this work, which uses a finite-dimensional Markov chain model, we consider an infinite-dimensional mean-field formulation where the equilibrium swarm density is the solution of a linear elliptic advection-diffusion PDE, which defines the equilibrium condition of the corresponding time-dependent parabolic problem. The feedback control law is the solution of a static Optimal Control Problem (OCP) whose state dynamics govern the equilibrium swarm density; the control field enters bilinearly into the state dynamics.

The dynamic version of this problem, where the state dynamics are described by an evolution equation in the form of a linear parabolic PDE, has been studied extensively; see, e.g., [10] for both theoretical and numerical treatments of the problem where the control field is null at the boundary, and [11] for a boundary control application. It is known that the dynamic control problem is controllable to every sufficiently smooth target distribution [12]. When a dynamic OCP is considered, the resulting control field is inherently open-loop and depends on the initial conditions. On the other hand, [13] stabilizes target distributions using a feedback control law that, although robust to external transient perturbations, is inversely proportional to the local swarm density, which generates unphysically large control fields when this density is close to zero. Moreover, the local density must be estimated by the agents using a communication mechanism that requires additional computational resources. A distributed algorithm for density estimation to reduce the computational cost is proposed in [14].

In the optimization-based algorithm that we propose here, the OCP is designed to compute an equilibrium swarm density that is as close as possible to a target density, which may be non-smooth, while balancing the control expenditure. The properties of the state operator enable us to show that the optimal control field globally stabilizes the equilibrium density, driving the swarm asymptotically to this density from every initial condition. In addition, our static approach is computationally efficient since it entails the solution of a static OCP at each iteration of a numerical optimization procedure. For cases where the initial swarm density is approximately known, we set up a dynamic OCP which makes use of the static solution. The dynamic OCP is formulated in a way that ensures convergence to the static, globally stabilizing control field. Based on properties of the infinite-dimensional formulation of the state system, we show the existence and uniqueness of the solution to the resulting OCP with a standard change of variables inspired by the literature on optimal transport (see, e.g., [15]), and we prove a stability theorem for the resulting equilibrium density.

From a computational standpoint, we propose a consistent finite-element discretization of both the transient and steady-state density dynamics and show that it preserves particular properties of the infinite-dimensional problem. Based on the kernel properties of the state matrix of the algebraic discretization, we develop a numerical algorithm to efficiently compute

the reduced gradient and the global minimum. The associated dynamic OCP is then solved in a similar way, using the static solution as a warm start. We also demonstrate that we are able to ensure convergence of the dynamic solution to the static solution of the OCP for both the state and control variables. This is a robustness property with respect to uncertainties in the initial conditions and transient disturbances. We validate our approach in numerical simulations that include complex scenarios in which the swarm moves through environments with obstacles and an external velocity field.

The paper is organized as follows. In Section II, the infinite-dimensional formulation of the OCP is presented and analyzed, and then optimality conditions are derived together with a set of useful properties. In Section III, the properties of the finite-element discretization of the OCP are proved and discussed in detail; a solution algorithm which exploits these properties is then proposed. In Section IV, three test cases are solved numerically to show the effectiveness of the proposed strategy. Some conclusions and directions for future work then follow in Section V.

II. THE OPTIMAL CONTROL PROBLEM

In this section, we formulate the density control problem both as a static OCP, which yields a time-independent control field that drives the swarm to a target equilibrium density, and as a modified dynamic OCP, which yields a time-varying control field that drives the swarm to this density within a specified time interval. After proving an existence and uniqueness result, we derive optimality conditions and prove some useful properties of the resulting system, including a global asymptotic stability result. Our modeling assumptions on the derivation of the macroscopic dynamics follow the same reasoning as in, e.g., [11] and [12], which we briefly review below.

We consider a swarm of robots, labeled $i = 1, \dots, N$, that move in a bounded domain $\Omega \in \mathbb{R}^2$. Robot i occupies position $\mathbf{X}_i(t) \in \Omega$ at time t and moves with controlled velocity $\mathbf{u}(\mathbf{x}, t) \in \mathbb{R}^2$. This motion is perturbed by a two-dimensional Wiener process $\mathbf{W}(t)$, which models stochasticity arising from inherent sensor and actuator noise or intentionally programmed “diffusive” exploratory behaviors. The robot’s position evolves according to the following Stochastic Differential Equation:

$$\begin{cases} d\mathbf{X}_i(t) = \mathbf{u}(\mathbf{X}_i, t)dt + \sqrt{2\mu}d\mathbf{W}(t) + \mathbf{n}(\mathbf{X}_i(t))d\psi(t) \\ \mathbf{X}_i(0) = \mathbf{X}_{i,0}, \end{cases}$$

where $\mu > 0$ is a diffusion coefficient, $\mathbf{n}(\mathbf{x})$ is the unit normal to the domain boundary at $\mathbf{x} \in \partial\Omega$, and $\psi(t) \in \mathbb{R}$ is a reflecting function, which ensures that the swarm does not exit the domain. The associated probability density $q(\mathbf{x}, t)$ satisfies the following linear parabolic PDE:

$$\frac{\partial q}{\partial t} + \nabla \cdot (-\mu \nabla q + \mathbf{u}q) = 0$$

complemented with no-flux boundary conditions. When considering a time-independent control field $\bar{\mathbf{u}}(\mathbf{x})$, the associated equilibrium density \bar{q} satisfies

$$\nabla \cdot (-\mu \nabla \bar{q} + \bar{\mathbf{u}}\bar{q}) = 0,$$

which is a homogeneous linear elliptic advection-diffusion PDE. Note that an integral constraint of the form $\int_{\Omega} \bar{q} d\Omega = 1$ has to be added to ensure that q represents a probability density, thus obtaining a well-posed problem with a nontrivial solution for each control action $\bar{\mathbf{u}}$. We can now formulate a static OCP as

$$\begin{aligned} J = \frac{\alpha}{2} \int_{\Omega} (\bar{q} - z)^2 d\Omega + \frac{\beta}{2} \int_{\Omega} \|\bar{\mathbf{u}}\|^2 d\Omega &\longrightarrow \min_{\bar{q}, \bar{\mathbf{u}}} \\ \text{s.t.} \\ \nabla \cdot (-\mu \nabla \bar{q} + \bar{\mathbf{u}} \bar{q}) = 0 &\quad \text{in } \Omega \\ (-\mu \nabla \bar{q} + \bar{\mathbf{u}} \bar{q}) \cdot \mathbf{n} = 0 &\quad \text{on } \partial\Omega \\ \int_{\Omega} \bar{q} d\Omega = 1 & \end{aligned} \quad (1)$$

where $\alpha, \beta > 0$ are control weighting constants, $z \in L^2(\Omega)$ is the target density, and $\bar{q} \in H^1(\Omega)$ is the equilibrium density, which constitutes the state of our OCP. In (1), $\bar{\mathbf{u}} \in L^\infty(\Omega)^2$ denotes the control field, which acts bilinearly on the state dynamics as an advection field. OCPs with integral state constraints are difficult to analyze and solve in general; however, in our case we can exploit the properties of the primal and dual problems to enforce the mass constraint effectively.

A. Analysis and functional setting

From here on, we will not use the overbar to denote static variables when it is clear from the context. The analysis of the state problem follows from an application of results from [16] that we can easily adapt to our case.

We define the infinite-dimensional family of fixed-mean subspaces as $\mathcal{M}_c = \{v \in H^1(\Omega) : \int_{\Omega} v d\Omega = c\} \subset H^1(\Omega)$. The weak formulation associated with the state problem (1) is: find $q \in \mathcal{M}_1$ such that

$$a(q, v; \mathbf{u}) = 0 \quad \forall v \in H^1(\Omega),$$

where the bilinear form a is defined as $a(q, v; \mathbf{u}) = \int_{\Omega} \mu \nabla q \cdot \nabla v - \mathbf{u} \cdot \nabla v q d\Omega$. By restricting our search for q to the space \mathcal{M}_1 , we obtain a well-posed problem. Indeed, the state solution belongs to the kernel of the operator $L_{\mathbf{u}} : H^1(\Omega) \mapsto H^1(\Omega)^*$ defined by

$$\langle L_{\mathbf{u}} q, v \rangle = a(q, v; \mathbf{u}),$$

restricted to $\mathcal{M}_1 \subset H^1(\Omega)$. In [16], it is proven that the kernel is one-dimensional and defined up to a multiplicative constant; as a consequence, the solution is unique in \mathcal{M}_1 for every control velocity field \mathbf{u} . Furthermore, it follows from the analysis in [16] that $q > 0$ a.e. on Ω and that the eigenvalues of the operator $L_{\mathbf{u}}$ are discrete and nonnegative, with the zero eigenvalue occurring with multiplicity one. Therefore, the eigenvalues of $L_{\mathbf{u}}$ when restricted to any \mathcal{M}_c , $c > 0$, are strictly positive. We will exploit this property to prove two stability theorems for the infinite-dimensional problem and its FEM discretized counterpart. We can now establish an existence and uniqueness result for the static OCP, exploiting the strict positivity of q .

Theorem 1 *The optimization problem (1) admits a unique global solution $\bar{\mathbf{u}}^* \in L^\infty(\Omega)^2$.*

PROOF Following [15], we can make the change of variables $\mathbf{m} = \bar{q} \bar{\mathbf{u}}$ and rewrite the problem (1) as:

$$\begin{aligned} J = \frac{\alpha}{2} \int_{\Omega} (\bar{q} - z)^2 d\Omega + \frac{\beta}{2} \int_{\Omega} \frac{1}{\bar{q}^2} \|\bar{\mathbf{m}}\|^2 d\Omega &\longrightarrow \min_{\bar{q}, \bar{\mathbf{m}}} \\ \text{s.t.} \\ -\mu \Delta \bar{q} = -\nabla \cdot (\bar{\mathbf{m}}) &\quad \text{in } \Omega \\ -\mu \nabla \bar{q} \cdot \mathbf{n} = \bar{\mathbf{m}} \cdot \mathbf{n} &\quad \text{on } \partial\Omega \\ \int_{\Omega} \bar{q} d\Omega = 1. & \end{aligned} \quad (2)$$

This is an infinite-dimensional convex optimization problem in the variables $\bar{\mathbf{m}}$ and \bar{q} , and as such it has a unique global minimum $\bar{\mathbf{m}}^*$, \bar{q}^* . We can then recover the optimal solution in the original variables as $\bar{\mathbf{u}}^* = \frac{\bar{\mathbf{m}}^*}{\bar{q}^*}$, since $q > 0$ a.e. on Ω .

The OCP formulation (1) does not include any weights on the spatial gradients of the control field. We will introduce a weight on these gradients in the cost functional such that the OCP yields a control field without steep gradients, in order to prevent control inputs whose variations are too large to be implemented on real robots. Note also that our stochastic single-integrator model will not accurately represent the microscopic dynamics of an individual robot if the control signal varies too quickly. Thus, we define an auxiliary regularized problem with identical dynamics and the following cost functional:

$$J_r = J + \frac{\beta_g}{2} \int_{\Omega} \|\nabla \mathbf{u}\|^2 d\Omega,$$

where $\beta_g > 0$ is the weight associated with the control gradients and $\|\nabla \mathbf{u}\|$ is the Frobenius norm of $\nabla \mathbf{u}$, defined

for every $\mathbf{x} \in \Omega$ as $\|\nabla \mathbf{u}(\mathbf{x})\| = \sqrt{\sum_{i=1}^2 \sum_{j=1}^2 \frac{\partial u_i(\mathbf{x})}{\partial x_j} \frac{\partial u_i(\mathbf{x})}{\partial x_j}}$. In the following remark, we sketch an equivalent formulation of the state dynamics.

Remark 1 (Equivalent formulation of the state dynamics) An equivalent way of proving the well-posedness of the state problem (1) is to make the change of variables $q = \dot{q} + \frac{1}{|\Omega|}$, where $|\Omega|$ is the measure of Ω . In this way, the integral constraint can be rewritten in terms of the new state variable \dot{q} as $\int_{\Omega} \dot{q} d\Omega = 0$, a homogeneous constraint. The dynamics of $\dot{q} \in H^1(\Omega)$ are therefore:

$$\begin{aligned} \nabla \cdot (-\mu \nabla \dot{q} + \mathbf{u} \dot{q}) &= -\frac{1}{|\Omega|} \nabla \cdot \mathbf{u} \quad \text{in } \Omega, \\ (-\mu \nabla \dot{q} + \mathbf{u} \dot{q}) \cdot \mathbf{n} &= -\frac{1}{|\Omega|} \mathbf{u} \cdot \mathbf{n} \quad \text{on } \partial\Omega, \\ \int_{\Omega} \dot{q} d\Omega &= 0. \end{aligned} \quad (3)$$

The integral constraint can be embedded into the weak formulation by selecting \mathcal{M}_0 as the functional space for both test and trial functions. The weak formulation of (3) then becomes: find $\dot{q} \in \mathcal{M}_0$ such that

$$\int_{\Omega} \mu \nabla \dot{q} \cdot \nabla v - \mathbf{u} \cdot \nabla v \dot{q} = \int_{\Omega} \frac{1}{|\Omega|} \mathbf{u} \cdot \nabla v \quad \forall v \in \mathcal{M}_0,$$

which can be proved to be well-posed by showing that it satisfies the hypotheses of the Nečas theorem (see, e.g., Theorem 6.6 in [17]), that is, continuity and weak coercivity

of the bilinear form on the left-hand side and continuity of the linear form on the right-hand side. In order to do so, it is useful to note that $\|\nabla v\|_{L^2(\Omega)}$ is a norm in \mathcal{M}_0 thanks to the generalized Poincaré inequality.

B. Optimality Conditions

Following a standard Lagrangian approach (see, e.g., [18]), we can recover a system of first-order necessary and sufficient optimality conditions for the static problem. Note that sufficiency is implied by the convexity of the transformed problem. We introduce the following Lagrangian functional:

$$\mathcal{L} = J - \int_{\Omega} \nabla \cdot (-\mu \nabla q + \mathbf{u} q) \lambda_q d\Omega + \lambda_m \left(\int_{\Omega} q d\Omega - 1 \right),$$

where $\lambda_q \in H^1(\Omega)$ is the multiplier function associated with the state constraint and $\lambda_m \in \mathbb{R}$ is the scalar multiplier associated with the conservation of mass constraint, which fixes the unique solution to the state problem (1). The adjoint equation can be obtained by setting the Gâteaux derivative of the Lagrangian functional with respect to a state variation to zero. Using integration by parts twice and substituting in the no-flux boundary conditions on the state dynamics (see, e.g., [11] for a detailed derivation), the adjoint equation reads:

$$\begin{aligned} -\mu \Delta \lambda_q - \mathbf{u} \cdot \nabla \lambda_q &= \alpha (q - z) + \lambda_m && \text{in } \Omega \\ \nabla \lambda_q \cdot \mathbf{n} &= 0 && \text{on } \partial\Omega \end{aligned}$$

Note that the adjoint/dual problem has a pure Neumann structure, so that we can select $\lambda_q \in \mathcal{M}_0$. It is also important to note that an explicit equation for the scalar multiplier λ_m is not given. However, it is shown in [16] that an additional condition on the right-hand side must hold,

$$\int_{\Omega} (\alpha (\bar{q} - z) + \lambda_m) \hat{v}_{\mathbf{u}} d\Omega = 0, \quad (4)$$

for $\hat{v}_{\mathbf{u}}$ in the kernel of the operator $L_{\mathbf{u}}$. Note that $q = a \hat{v}_{\mathbf{u}}$, where $a \in \mathbb{R}$ is fixed by q being a probability density. Hence, the right-hand side of the adjoint equation must be orthogonal to the state. This condition is preserved by the FEM discretization and will be used to compute λ_m . The Euler equation is obtained by setting the Gâteaux derivative of the Lagrangian functional with respect to a vector control variation to zero. Following a procedure similar to the adjoint derivation, we obtain:

$$-\beta_g \Delta \mathbf{u} + \beta \mathbf{u} + \nabla \lambda_q q = 0. \quad (5)$$

The optimal control for $\beta_g = 0$ has interesting properties, which we prove in the following proposition.

Proposition 1 (Structure of the optimal control) *The unique optimal control solution \mathbf{u}^* of the OCP (1) is tangent to the boundary $\partial\Omega$ of the domain Ω .*

PROOF The optimal control solves the Euler equation (5). Therefore, $\mathbf{u}^* = -\frac{1}{\beta} \nabla \lambda_q^* q^*$, where λ_q^* solves the adjoint equation so that we have:

$$\mathbf{u}^* \cdot \mathbf{n} = -\frac{1}{\beta} \nabla \lambda_q^* q^* \cdot \mathbf{n} = 0 \quad \text{on } \partial\Omega$$

due to the adjoint boundary conditions.

The boundary condition on the optimal control enables the density dynamics to avoid obstacles. This provides an advantage over density control laws that only depend on the target density z , and thus cannot have this property.

We are now ready to formulate the associated dynamic OCP on a time interval $[0, T]$, where T denotes both the final time and the width of the interval, without loss of generality. It is known that for sufficiently large T , both the infinite-dimensional formulation of this kind of problem and, consistently, its discrete FEM formulation exhibit the so-called *turnpike behavior* [19], [20]. In other words, the dynamics of the optimal state, adjoint, and control triple will progress through three stages: first, a transient stage that is determined by the initial conditions; then, a “steady-state” stage in which the optimal triple is approximately constant and asymptotically close to an equivalent static OCP; and finally, another transient stage that is determined by the terminal conditions.

In our setting, it is natural to require the optimal solution of the dynamic problem to converge to its static counterpart. In this way, if the initial conditions are known, we can speed up the transient to the optimal equilibrium density. Thanks to the turnpike property, it is then sufficient to set the cost functional for the dynamic problem as:

$$\begin{aligned} J_t = & \frac{\alpha}{2} \int_0^T \int_{\Omega} (q - \bar{q}^*)^2 dt d\Omega + \frac{\beta}{2} \int_0^T \int_{\Omega} \|\mathbf{u} - \bar{\mathbf{u}}^*\|^2 dt d\Omega \\ & + \frac{\beta_g}{2} \int_0^T \int_{\Omega} \|\nabla(\mathbf{u} - \bar{\mathbf{u}}^*)\|^2 dt d\Omega \end{aligned}$$

with state dynamics:

$$\begin{aligned} \frac{\partial q}{\partial t} + \nabla \cdot (-\mu \nabla q + \mathbf{u} q) &= 0 && \text{in } \Omega \times (0, T) \\ (-\mu \nabla q + \mathbf{u} q) \cdot \mathbf{n} &= 0 && \text{on } \partial\Omega \times (0, T) \\ q(\mathbf{x}, 0) &= q_0(\mathbf{x}) && \text{on } \Omega \times \{0\} \end{aligned} \quad (6)$$

and the additional box constraint $|\mathbf{u}(\mathbf{x}, t)| \leq \|\bar{\mathbf{u}}^*\|_{L^{\infty}(\Omega)^2}$ for every $\mathbf{x} \in \Omega$ and a.e. on $t \in (0, T)$, which ensures that the dynamic control action has the same magnitude as its static counterpart, in an L^{∞} sense.

The adjoint equation for this modified dynamic problem is:

$$\begin{aligned} -\frac{\partial \lambda_q}{\partial t} - \mu \Delta \lambda_q - \mathbf{u} \cdot \nabla \lambda_q &= \alpha (q - \bar{q}^*) && \text{in } \Omega \times (0, T) \\ \nabla \lambda_q \cdot \mathbf{n} &= 0 && \text{on } \partial\Omega \times (0, T) \\ \lambda_q(\mathbf{x}, T) &= 0 && \text{on } \Omega \times \{T\}, \end{aligned}$$

while the Euler equation or reduced gradient can be written as

$$\nabla J = -\beta_g \Delta(\mathbf{u} - \bar{\mathbf{u}}^*) + \beta(\mathbf{u} - \bar{\mathbf{u}}^*) + \nabla \lambda_q q. \quad (7)$$

An important property of the state system (6) is that it is mass-conservative, which is required given that the state q is a probability density. It is easy to show this property: defining $m(t) = \int_{\Omega} q(\mathbf{x}, t) d\Omega$, we have that:

$$\begin{aligned} \dot{m} &= \int_{\Omega} \frac{\partial q}{\partial t} d\Omega \\ &= - \int_{\Omega} \nabla \cdot (-\mu \nabla q + \mathbf{u} q) d\Omega = \int_{\partial\Omega} (-\mu \nabla q + \mathbf{u} q) \cdot \mathbf{n} d\Omega = 0. \end{aligned} \quad (8)$$

In the following, we will show that the FEM discretization is consistent with this property. The mass-preserving property of the state equation can be interpreted as forward invariance with respect to the subspace \mathcal{M}_1 . Note that the usual zero-mean subspace is \mathcal{M}_0 . Note also that the integral constraint on the density q need not be taken into account explicitly, due to the mass-preserving property of the state equation and the fact that $q_0 \in \mathcal{M}_1$. Another fundamental property of the density dynamics (6) is that the state solution is nonnegative, that is, $q(t) \geq 0$ for a.e. $t \in (0, T)$; see, e.g., [12] for a semigroup-theoretic approach to proving this property.

Moreover, for a sufficiently large time interval $(0, T)$, the turnpike property implies that after a transient due to the initial conditions, $\mathbf{u}^*(t) \rightarrow \bar{\mathbf{u}}^*$ and $q^*(t) \rightarrow \bar{q}^*$. This can be interpreted as a robustness property: even if the initial conditions are not exactly known, the convergence to the optimal steady-state control action still ensures convergence to the target density, since the equilibrium induced by $\bar{\mathbf{u}}^*$ is globally asymptotically stable. The global asymptotic stability of this equilibrium is established by the following theorem.

Theorem 2 *The unique optimal solution $\bar{q}^*(\bar{\mathbf{u}}^*)$ of problem (1) is globally asymptotically stable on the mass-preserving subspace \mathcal{M}_1 .*

PROOF Existence and uniqueness of $\bar{q}^*(\bar{\mathbf{u}}^*)$ follows from Theorem 1. To show global asymptotic stability, consider the Lyapunov function $\mathcal{V} = \frac{1}{2} \int_{\Omega} (q - \bar{q}^*)^2 d\Omega$. Define the error $e := q - \bar{q}^*$ and note that $e \in \mathcal{M}_0$. \mathcal{V} is positive on \mathcal{M}_0 and vanishes only for $q = \bar{q}^*$. The time derivative of \mathcal{V} along the solution of the state equation is:

$$\begin{aligned} \dot{\mathcal{V}} &= \int_{\Omega} e \frac{\partial q}{\partial t} d\Omega = - \int_{\Omega} e \nabla \cdot (-\mu \nabla q + \bar{\mathbf{u}}^* q) d\Omega \\ &= - \int_{\Omega} e \nabla \cdot (-\mu \nabla e + \bar{\mathbf{u}}^* e) d\Omega \\ &= - \int_{\Omega} (\mu \|\nabla e\|^2 - \bar{\mathbf{u}}^* \cdot \nabla e e) d\Omega = - \langle L_{\bar{\mathbf{u}}^*} e, e \rangle, \end{aligned}$$

where we have substituted the steady-state condition $\nabla \cdot (-\mu \bar{q}^* + \bar{\mathbf{u}}^* \bar{q}) = 0$ and the no-flux boundary conditions. Now, the final expression of $\dot{\mathcal{V}}$ is a weak formulation associated with the state operator, and it is formulated on \mathcal{M}_0 . It is proven in [16] that this operator is strictly positive on this subspace, and thus $\dot{\mathcal{V}} < 0$.

In the next section, we will prove that the FEM discretization inherits the properties of the associated infinite-dimensional formulation, and thus a stability proof for the semi-discrete system can use arguments similar to Theorem 2 but in a finite-dimensional, algebraic setting.

III. NUMERICAL ANALYSIS OF THE OCP

In this section, we analyse the FEM discretization of both the static and dynamic OCPs and propose numerical algorithms for their solutions that are based on the algebraic properties of the finite-dimensional problem. The FEM discretization inherits the structure of the infinite-dimensional problem and, in particular, the state dynamics reduce to a

kernel-finding problem with a unique solution determined by the discretized integral mass constraint.

In the static problem, the FEM discretization of the state dynamics is

$$\begin{aligned} (A - \mathbb{B}_x^\top \mathbf{u}_x - \mathbb{B}_y^\top \mathbf{u}_y) \mathbf{q} &= \mathbf{0}, \\ \mathbf{F}^\top \mathbf{q} - 1 &= \mathbf{0}; \end{aligned} \quad (9)$$

the adjoint dynamics are given by

$$(A - \mathbb{B}_x \mathbf{u}_x - \mathbb{B}_y \mathbf{u}_y) \boldsymbol{\lambda}_q = \alpha M(\mathbf{q} - \mathbf{z}) + \lambda_m \mathbf{F}; \quad (10)$$

and the Euler equation can be expressed as

$$\begin{aligned} \beta M_u \mathbf{u}_x + \beta_g A_u \mathbf{u}_x + \boldsymbol{\lambda}_q^\top \mathbb{B}_x \mathbf{q} &= \mathbf{0}, \\ \beta M_u \mathbf{u}_y + \beta_g A_u \mathbf{u}_y + \boldsymbol{\lambda}_q^\top \mathbb{B}_y \mathbf{q} &= \mathbf{0}. \end{aligned}$$

In these equations, A and M are the usual stiffness and mass matrices, while \mathbb{B}_x is a rank-3 tensor defined as $\mathbb{B}_{x,ijk} = \int_{\Omega} \frac{\partial \phi_i}{\partial x} \phi_j \phi_k d\Omega$ and \mathbb{B}_y is defined in a similar way. For an alternative and equivalent way of defining the FEM matrices, see [11]. The vectors \mathbf{q} , \mathbf{z} , $\boldsymbol{\lambda}_q \in \mathbb{R}^{N_q}$ denote the coefficients of the FEM basis functions for the state, target, and adjoint variables, respectively. The entries of the vector $\mathbf{F} \in \mathbb{R}^{N_q}$ are defined as $\mathbf{F}_i = \int_{\Omega} \phi_i d\Omega$, where ϕ_i is the corresponding FEM basis function. Given this definition, the mass of an FEM variable $v_h = \sum_{i=1}^N \phi_i v_i$ is simply:

$$\int_{\Omega} v_h d\Omega = \sum_{i=1}^N \int_{\Omega} \phi_i d\Omega v_i = \mathbf{F}^\top \mathbf{v}.$$

With a slight abuse of notation, we group the FEM discretizations of the x and y components of the control action as $\mathbf{u} = [\mathbf{u}_x \ \mathbf{u}_y]^\top$ and define $\mathbb{B} = \text{Stack3}(\mathbb{B}_x, \mathbb{B}_y)$, where the `Stack3` operation stacks \mathbb{B}_x and \mathbb{B}_y along the third direction. In this way, we can compactly write

$$\mathbb{B} \mathbf{u}_x + \mathbb{B}_y \mathbf{u}_y = \mathbb{B} \mathbf{u};$$

note that $\mathbb{B} \mathbf{u}$ is a matrix. The transpose operation on \mathbb{B} is defined as $\mathbb{B}_{ijk}^\top = \mathbb{B}_{jik}$. The transpose of the state matrix, $A - \mathbb{B} \mathbf{u}$, can be easily seen to be the discrete adjoint matrix, A being symmetric. This, in turn, implies full commutativity of the Discretize-then-Optimize (DtO) and Optimize-then-Discretize (OtD) solution methods for this problem; see [11] and [18, Ch. 6], for more details.

The semi-discrete set of modified optimality conditions arising from the discretization (in space) of the dynamic problem is:

$$\begin{aligned} M \dot{\mathbf{q}} + (A - \mathbb{B}^\top \mathbf{u}) \mathbf{q} &= \mathbf{0}, \quad t \in (0, T) \\ \mathbf{q}(0) &= \mathbf{q}_0; \end{aligned} \quad (11a)$$

$$\begin{aligned} -M \dot{\boldsymbol{\lambda}}_q + (A - \mathbb{B} \mathbf{u}) \boldsymbol{\lambda}_q &= \alpha M_q (\mathbf{q} - \bar{\mathbf{q}}^*), \quad t \in (0, T) \\ \boldsymbol{\lambda}_q(T) &= \mathbf{0}; \end{aligned} \quad (11b)$$

$$(\beta M_u + \beta_g A_u) (\mathbf{u}_x - \bar{\mathbf{u}}_x^*) + \boldsymbol{\lambda}_q^\top \mathbb{B}_x^\top \mathbf{q} = \mathbf{0}, \quad t \in (0, T)$$

$$(\beta M_u + \beta_g A_u) (\mathbf{u}_y - \bar{\mathbf{u}}_y^*) + \boldsymbol{\lambda}_q^\top \mathbb{B}_y^\top \mathbf{q} = \mathbf{0}, \quad t \in (0, T)$$

where we have used the definition of \mathbb{B} to compactly write both the state and adjoint dynamics. We remark that in the static problem, we solve for a constant vector $\bar{\mathbf{u}} \in \mathbb{R}^{2N_u}$, while in the dynamic problem, our unknowns $\mathbf{q} = \mathbf{q}(t), \mathbf{u} = \mathbf{u}(t)$ are time-dependent.

A. Properties of FEM discretization

We define the mass-preserving linear subspace arising from the FEM discretization as $\tilde{\mathcal{M}}_c = \{\mathbf{v} \in \mathbb{R}^{N_q} : \mathbf{F}^\top \mathbf{v} = c\}$ for some total mass $c > 0$. In the following, we will need in particular $\tilde{\mathcal{M}}_0$ and $\tilde{\mathcal{M}}_1$; note the close parallel with their infinite-dimensional counterparts \mathcal{M}_0 and \mathcal{M}_1 . We can now prove a number of useful properties that the FEM approximation inherits from the infinite-dimensional problem, thus making it a consistent (and elegant) discretization of the OCP.

Proposition 2 *For each $\mathbf{u} \in \mathbb{R}^{2N_u}$, $\mathbf{1} \in \text{Ker}(A - \mathbb{B}\mathbf{u})$ and the dimension of $\text{Ker}(A - \mathbb{B}\mathbf{u})$ is 1; that is, $\text{Span}(\text{Ker}(A - \mathbb{B}^\top \mathbf{u})) = \{\mathbf{1}\}$.*

PROOF The matrix $A - \mathbb{B}\mathbf{u}$ is the FEM discretization of the adjoint PDE operator, which is defined up to a constant since the adjoint system is a pure Neumann problem. In FEM terms, this constant corresponds to the vector $\mathbf{1} \in \mathbb{R}^{N_q}$; see, e.g., [21].

From Proposition 2, a simple yet useful result follows for the discretized state problem, also ensuring its well-posedness. This result is stated in the following proposition.

Proposition 3 *The kernel of the state matrix $(A - \mathbb{B}^\top \mathbf{u})$ is one-dimensional, that is, $\text{Dim}(\text{Ker}(A - \mathbb{B}^\top \mathbf{u})) = 1 \forall \mathbf{u} \in \mathbb{R}^{2N_u}$.*

PROOF $\text{Rank}(A - \mathbb{B}^\top \mathbf{u}) = \text{Rank}(A - \mathbb{B}\mathbf{u}) = N_q - 1$, and thus $\text{Dim}(\text{Ker}(A - \mathbb{B}^\top \mathbf{u})) = 1$.

We denote the vector spanning the kernel of $A - \mathbb{B}^\top \mathbf{u}$ as $\mathbf{v}(\mathbf{u})$ and note that the kernel of $A - \mathbb{B}\mathbf{u}$ is spanned by the vector of ones, $\mathbf{1}$, for every control action $\mathbf{u} \in \mathbb{R}^{2N_u}$. The previous results allow us to prove the following proposition regarding the mass-preserving property of the semi-discrete system.

Proposition 4 *The FEM discretization of the state equation in the dynamic OCP,*

$$\begin{aligned} M\dot{\mathbf{q}} + (A - \mathbb{B}^\top \mathbf{u})\mathbf{q} &= \mathbf{0}, \quad t \in (0, T) \\ \mathbf{q}(0) &= \mathbf{q}_0, \end{aligned}$$

is mass-conservative with respect to the FEM mass function $m_d(t) = \int_{\Omega} \sum_{i=1}^{N_q} \phi_i q_i d\Omega = \mathbf{F}^\top \mathbf{q}$. That is, $\dot{m}_d = 0$ for every control action \mathbf{u} .

PROOF We can use the relation $\mathbf{F} = M\mathbf{1}$ (see, e.g., [21]), Proposition 2, and the semi-discrete state dynamics to obtain:

$$\dot{m}_d = \mathbf{F}^\top \dot{\mathbf{q}} = \mathbf{1}^\top M\dot{\mathbf{q}} = -\mathbf{1}^\top (A - \mathbb{B}^\top \mathbf{u})\mathbf{q} = 0.$$

Proposition 4 constitutes the finite-dimensional analogue of Equation (8). In other words, by choosing $\mathbf{q}_0 \in \tilde{\mathcal{M}}_1$, we have that $\mathbf{q}(t) \in \tilde{\mathcal{M}}_1$ for a.e. $t \in (0, T)$, which means that the linear subspace $\tilde{\mathcal{M}}_1$ is forward invariant for the semi-discrete dynamics. We are now ready to prove a useful stability

theorem which ensures that for every control action $\bar{\mathbf{u}}$, the resulting equilibrium is unique and globally asymptotically stable on the relative mass-preserving subspace, which we assume to be $\tilde{\mathcal{M}}_1$. Without loss of generality, we prove this result for the equilibrium density induced by the optimal control $\bar{\mathbf{u}}^*$.

Theorem 3 *The optimal equilibrium density $\bar{\mathbf{q}}^*(\bar{\mathbf{u}}^*)$ is unique and globally asymptotically stable.*

PROOF Since $\text{Dim}(\text{Ker}(A - \mathbb{B}^\top \bar{\mathbf{u}}^*)) = 1$, the equilibrium density has the form $\bar{\mathbf{q}}^*(\bar{\mathbf{u}}^*) = k\mathbf{v}(\bar{\mathbf{u}}^*)$, where $\mathbf{v}(\bar{\mathbf{u}}^*)$ is the vector spanning the one-dimensional kernel of the state dynamics and $k \in \mathbb{R}$ has to be determined. Imposing the condition $\bar{\mathbf{q}}^* \in \tilde{\mathcal{M}}_1$, that is $\mathbf{F}^\top \bar{\mathbf{q}}^*(\bar{\mathbf{u}}^*) = 1$, we obtain a unique solution.

The bilinear form $a(q, v; \mathbf{u})$ that arises from the weak formulation of the state equation is associated with an operator with nonnegative eigenvalues when q, v belong to the zero-mean space. We proved that the FEM solution $\mathbf{q}(t)$ remains on the mass-preserving subspace $\tilde{\mathcal{M}}_1$. Defining $B \in \mathbb{R}^{N_q \times N_q-1}$ as a basis for $\tilde{\mathcal{M}}_0 \subset \mathbb{R}^{N_q}$, there exist vectors $\bar{\mathbf{w}}(t), \bar{\mathbf{w}}^* \in \mathbb{R}^{N_q-1}$ such that $\dot{\mathbf{q}}(t) = B\bar{\mathbf{w}}(t)$ and $\bar{\mathbf{q}}^* = B\bar{\mathbf{w}}^* + \frac{1}{|\Omega|}\mathbf{1}$. Furthermore, since the FEM approximation selects $q_h, v_h \in V_h \subset H^1(\Omega)$, the strict positivity of the operator on the mass-preserving subspace implies that:

$$a(v_h, v_h; \bar{\mathbf{u}}^*) = \mathbf{v}^\top B^\top (A - \mathbb{B}^\top \bar{\mathbf{u}}^*) B \mathbf{v} > 0$$

for every $\mathbf{v} \in \mathbb{R}^{N_q-1}$. Now, consider the candidate Lyapunov function $l(\mathbf{q}) = \frac{1}{2}(\mathbf{q} - \bar{\mathbf{q}}^*)^\top M(\mathbf{q} - \bar{\mathbf{q}}^*)$. It is clear that $l > 0 \quad \forall \mathbf{q} \neq \bar{\mathbf{q}}^*$, since the mass matrix M is positive definite. Using the previous results, we show that $\dot{l} < 0$ along solutions of the semi-discrete FEM dynamics $M\dot{\mathbf{q}} + (A - \mathbb{B}^\top \bar{\mathbf{u}}^*)\mathbf{q} = \mathbf{0}$. Indeed, since the bilinear form $a(q, v; \mathbf{u})$ is strictly positive on $\mathcal{M}_0, \tilde{\mathcal{M}}_0 \subset \mathcal{M}_0$ and $\mathbf{q}(t) - \bar{\mathbf{q}}^* = B\mathbf{w}(t)$ for some $\mathbf{w}(t) \in \mathbb{R}^{N_q-1}$, we have that

$$\begin{aligned} \dot{l} &= (\mathbf{q} - \bar{\mathbf{q}}^*)^\top M\dot{\mathbf{q}} \\ &= -(\mathbf{q} - \bar{\mathbf{q}}^*)^\top (A - \mathbb{B}^\top \bar{\mathbf{u}}^*)\mathbf{q} \\ &= -(\mathbf{q} - \bar{\mathbf{q}}^*)^\top (A - \mathbb{B}^\top \bar{\mathbf{u}}^*)(\mathbf{q} - \bar{\mathbf{q}}^*) \\ &= -\mathbf{w}^\top B^\top (A - \mathbb{B}^\top \bar{\mathbf{u}}^*) B \mathbf{w} < 0. \end{aligned}$$

Note that it is not unexpected that the finite-dimensional stability proof mirrors the steps of its infinite-dimensional counterpart (Theorem 2), since the FEM discretization inherits the properties of the associated infinite-dimensional operators.

When solving the dynamic OCP, a consistent discretization in time is needed. The so-called θ -method (see, e.g., [18, Ch. 8]) for semi-discrete evolution problems reads, in our case,

$$\begin{aligned} \frac{M}{\Delta t}(\mathbf{q}_{i+1} - \mathbf{q}_i) + \theta(A - \mathbb{B}^\top \mathbf{u}_{i+1})\mathbf{q}_{i+1} \\ + (1 - \theta)(A - \mathbb{B}^\top \mathbf{u}_i)\mathbf{q}_i &= \mathbf{0}, \quad i = 0, \dots, N_t - 1 \\ \mathbf{q}_0 &\text{ given} \end{aligned} \tag{12}$$

where Δt is the time step, N_t is the number of time discretization points, and $\theta \in [0, 1]$ is selected by the user. The choice of $\theta = 0$ and $\theta = 1$ gives the classical forward and backward Euler methods, respectively. It can also be proven

that the only method of order 2 in time is the Crank-Nicolson method, which is obtained by selecting $\theta = \frac{1}{2}$; see, e.g., [22, Ch. 5]. Note that \mathbf{q}_0 is set equal to the initial condition. A straightforward application of Proposition 2 allows us to prove that the full discretization using a θ -method remains mass-preserving.

Proposition 5 *The θ -method time discretization is mass-preserving. That is, if $\mathbf{q}_i \in \tilde{\mathcal{M}}_1$, then $\mathbf{q}_{i+1} \in \tilde{\mathcal{M}}_1$ as well, or equivalently,*

$$\mathbf{F}^\top(\mathbf{q}_{i+1} - \mathbf{q}_i) = 0.$$

PROOF Since $\mathbf{1}$ is in the kernel of $(A - \mathbb{B}^\top \mathbf{u})$ for every $\mathbf{u} \in \mathbb{R}^{2N_u}$, we can use the same arguments as in Proposition 4 to obtain:

$$\begin{aligned} \mathbf{F}^\top(\mathbf{q}_{i+1} - \mathbf{q}_i) &= \mathbf{1}^\top M(\mathbf{q}_{i+1} - \mathbf{q}_i) \\ &= -\Delta t \theta \mathbf{1}^\top (A - \mathbb{B}^\top \mathbf{u}_{i+1}) \mathbf{q}_{i+1} \\ &\quad - \Delta t (1 - \theta) \mathbf{1}^\top (A - \mathbb{B}^\top \mathbf{u}_i) \mathbf{q}_i = 0. \end{aligned}$$

In other words, Proposition 5 states that the increment is orthogonal to the FEM mass vector \mathbf{F} , and thus the discrete evolution of \mathbf{q}_i remains in the mass-preserving subspace for all $i = 0, \dots, N_t$ and for every control action \mathbf{u}_i , which may be time-varying.

The last step of our numerical analysis is to ensure that the numerical solution \mathbf{q}_i remains nonnegative for every $i = 1, \dots, N_t$, given that $\mathbf{q}_0 \geq \mathbf{0}$. In order to rigorously prove this property *a priori* for a fully discrete scheme, a discrete form of the maximum principle needs to be proved. Positivity is ensured if the stiffness matrix resulting from the FEM discretization is an M-matrix (see, e.g., [23], [24]) and the mass lumping technique is used together with, for example, a backward Euler method [25], [24]. Modified finite-element schemes are available to ensure these properties under mild assumptions on the geometry of the finite element mesh, see, e.g., [24], [26]. However, for sufficiently fine meshes of strict Delaunay type, the standard FEM together with the mass lumping technique is positivity preserving (see [24], [26], [27]). For the sake of simplicity, here we use a standard Galerkin method with mass lumping, making sure that the FEM mesh satisfies the geometric assumptions that ensure positivity preservation. We remark that in each of our numerical test cases, the density remains nonnegative throughout all optimization iterations.

B. Solution algorithm

Exploiting the properties of the algebraic systems governing the state and adjoint variables, we can derive a numerical algorithm to compute the reduced gradient. The main difficulty is to find the Lagrange multiplier λ_m associated with the mass constraint. By projecting the discrete adjoint equation on the kernel of the state equation, we can recover an equation for λ_m . Then, some care is needed in the numerical treatment of the adjoint system. Since it results from the discretization of a pure Neumann problem, the adjoint problem comprises a singular system with a one-dimensional kernel spanned by $\mathbf{1}$ [21]. This, in turn, means that its solution is defined up to an arbitrary constant. Following [21], a more robust way

Algorithm 1 Reduced gradient computation with integral density constraint

- 1: $\mathbf{v}(\mathbf{u}) \leftarrow \text{Span}(\text{Ker}(A - \mathbb{B}^\top \mathbf{u}))$ ▷ Solve state equation (9)
- 2: $\mathbf{q} \leftarrow \frac{\mathbf{v}(\mathbf{u})}{\mathbf{F}^\top \mathbf{v}(\mathbf{u})}$
- 3: $\lambda_m \leftarrow -\frac{\alpha \mathbf{v}(\mathbf{u})^\top M_q(\mathbf{q} - \mathbf{z})}{\mathbf{v}(\mathbf{u})^\top \mathbf{F}}$
- 4: $\boldsymbol{\lambda}_q \leftarrow \text{Solve Problem (13)}$
- 5: $\nabla_{\mathbf{u}_x} \tilde{J} = \beta M_u \mathbf{u}_x + \boldsymbol{\lambda}_q^\top \mathbb{B}_x^\top \mathbf{q}$ ▷ Compute reduced gradient
- 6: $\nabla_{\mathbf{u}_y} \tilde{J} = \beta M_u \mathbf{u}_y + \boldsymbol{\lambda}_q^\top \mathbb{B}_y^\top \mathbf{q}$

to solve the adjoint system is to look for solutions which have zero mean. In the infinite-dimensional formulation, this amounts to requiring that $\int_{\Omega} \lambda_q d\Omega = 0$, which in the FEM discretization readily translates to $\mathbf{F}^\top \boldsymbol{\lambda}_q = 0$. Note the duality with the state system, which should satisfy $\mathbf{F}^\top \mathbf{q} = 1$. For the sake of brevity, we just provide the FEM discretization of the optimization problem whose solution provides the adjoint system. An associated variational formulation in continuous space can also be derived (see, e.g., [21]). For fixed controls, the adjoint solution solves the linearly constrained, quadratic optimization problem:

$$\begin{aligned} \frac{1}{2} \boldsymbol{\lambda}_q^\top (A - \mathbb{B} \mathbf{u}) \boldsymbol{\lambda}_q - \left(\alpha M_q(\mathbf{q} - \mathbf{z}) + \lambda_m \mathbf{F} \right)^\top \boldsymbol{\lambda}_q &\longrightarrow \min_{\boldsymbol{\lambda}_q} \\ \text{s.t. } \mathbf{F}^\top \boldsymbol{\lambda}_q &= 0 \end{aligned} \tag{13}$$

where λ_m can be computed using the kernel properties of the state system and the adjoint system. The KKT system arising from Problem (13) is a well-posed sparse linear system. The numerical computation of the reduced gradient is sketched in Algorithm 1.

The explicit computation of λ_m in Algorithm 1 utilizes the kernel properties of the state matrix. Left-multiplying the adjoint equation (10) by $\mathbf{v}(\mathbf{u})$, and applying the result in Proposition 3, we obtain

$$\alpha \mathbf{v}(\mathbf{u})^\top M(\mathbf{q} - \mathbf{z}) + \lambda_m \mathbf{v}(\mathbf{u})^\top \mathbf{F} = \mathbf{v}(\mathbf{u})^\top (A - \mathbb{B} \mathbf{u}) \boldsymbol{\lambda}_q = 0,$$

which can be used to compute λ_m . Note that this condition ensures the well-posedness of the adjoint equation and corresponds to Equation (4).

In order to compute the solution to the static optimization problem, we use the quasi-Newton method outlined in Algorithm 2. In this method, the reduced Hessian is approximated by a matrix of the form $\beta M_u + \beta_g A_u$. Note that this matrix is not the FEM equivalent of the reduced Hessian, which is both harder to derive and more difficult to compute. For a derivation of second-order necessary conditions for a similar problem, see [28]; an alternative numerical treatment based on the conjugate gradient method, which does not require the computation of the reduced Hessian, can be found in [29]. The dynamic problem is solved with a similar iterative quasi-Newton method, whose steps are sketched in Algorithm 3. We illustrate the properties of the discretized OCP in Figure 1.

Algorithm 2 Modified Newton method for static OCP

```

1:  $H \leftarrow \beta M_u + \beta_g A_u$ 
2: for  $i = 0$  : maxIter do
3:    $\nabla J(\mathbf{u}^{(i)}) \leftarrow \text{Algorithm1}(\mathbf{u}^{(i)})$      $\triangleright$  Compute reduced
   gradient
4:    $\mathbf{d}^{(i)} \leftarrow \text{Solve } H\mathbf{d}^{(i)} = -\nabla J(\mathbf{u}^{(i)})$ 
5:    $\tau \leftarrow \text{ArmijoBacktracking}(J, \mathbf{d}^{(i)}, \mathbf{u}^{(i)})$      $\triangleright$  Line search
6:    $\mathbf{u}^{(i+1)} \leftarrow \mathbf{u}^{(i)} + \tau \mathbf{d}^{(i)}$      $\triangleright$  Update control
7:   if  $\|\nabla J(\mathbf{u}^{(i)})\| < \text{tol}$  then
8:     return
9:   end if
10:  end for

```

Algorithm 3 Modified Newton method for dynamic OCP

```

1:  $H \leftarrow \beta M_u + \beta_g A_u$ 
2:  $\bar{\mathbf{q}}^*, \bar{\mathbf{u}}^*, \bar{\lambda}^* \leftarrow \text{Algorithm2}$      $\triangleright$  Solve static OCP
3:  $\mathbf{u}^0 \leftarrow \text{Repmat}(\bar{\mathbf{u}}^*, N_t)$      $\triangleright$   $N_t$  copies of solution to static
   OCP
4: for  $i = 0$  : maxIter do
5:    $\mathbf{q}^{(i)} \leftarrow \text{SolveStateDyn}(\mathbf{u}^{(i)})$      $\triangleright$  Solve Eq. (11a)
6:    $\lambda_q^{(i)} \leftarrow \text{SolveAdjointDyn}(\mathbf{u}^{(i)}, \mathbf{q}^{(i)}, \bar{\mathbf{q}}^*)$      $\triangleright$  Solve Eq.
   (11b)
7:    $\nabla J(\mathbf{u}^{(i)}) \leftarrow H(\mathbf{u}^{(i)} - \bar{\mathbf{u}}^*) + \lambda_q^{(i)\top} \mathbb{B}^\top \mathbf{q}^{(i)}$ 
8:    $\mathbf{d}^{(i)} \leftarrow \text{Solve } H\mathbf{d}^{(i)} = -\nabla J(\mathbf{u}^{(i)})$ 
9:    $\tau \leftarrow \text{ArmijoBacktracking}(J, \mathbf{d}^{(i)}, \mathbf{u}^{(i)})$      $\triangleright$  Line search
10:   $\mathbf{u}^{(i+1)} \leftarrow \mathbf{u}^{(i)} + \tau \mathbf{d}^{(i)}$      $\triangleright$  Update control
11:  if  $\|\nabla J(\mathbf{u}^{(i)})\| < \text{tol}$  then
12:    return
13:  end if
14:  end for

```

IV. NUMERICAL SIMULATIONS

In this section, we show the effectiveness of our control algorithm through numerical simulations of three test cases. In all cases, the computational domain is discretized into a triangular mesh with N_q degrees of freedom, and the time interval $[0, T]$ is discretized into time steps $\Delta t = 0.03$ [s], where $T = 3$ [s]. Test case 2 is also run for $T = 100$ [s] with the control field $\bar{\mathbf{u}}^*$ from the static OCP only. The resulting fully discrete optimization problem has N_q state variables and $2N_q$ control variables in the static case, while in the dynamic case the number of variables is multiplied by N_t . We set $N_q = 2704$ in test case 1, $N_q = 2603$ in test case 2, and $N_q = 3831$ in test case 3. Computations are carried out in MATLAB using a modified version of the `redBKIT` library [30] to assemble the FEM matrices and tensors and the `TensorToolbox` [31] to perform efficient tensor computations.

In test case 1, we define the domain as $\Omega = [-1, 1]^2 \setminus B(\mathbf{0}, 0.2)$, where $B(\mathbf{x}, r)$ denotes the two-dimensional ball centered at \mathbf{x} with radius r . The ball $B(\mathbf{0}, 0.2)$ represents a circular obstacle which must be avoided by the density dynamics. Figure 2 plots the target density z and the numerical solution of the static optimization problem, comprised of the equilibrium density \bar{q}^* and control field $\bar{\mathbf{u}}^*$, along with the norm of $\bar{\mathbf{u}}^*$. The plots show that the equilibrium density is smooth, non-negative, and close to the target density, and that

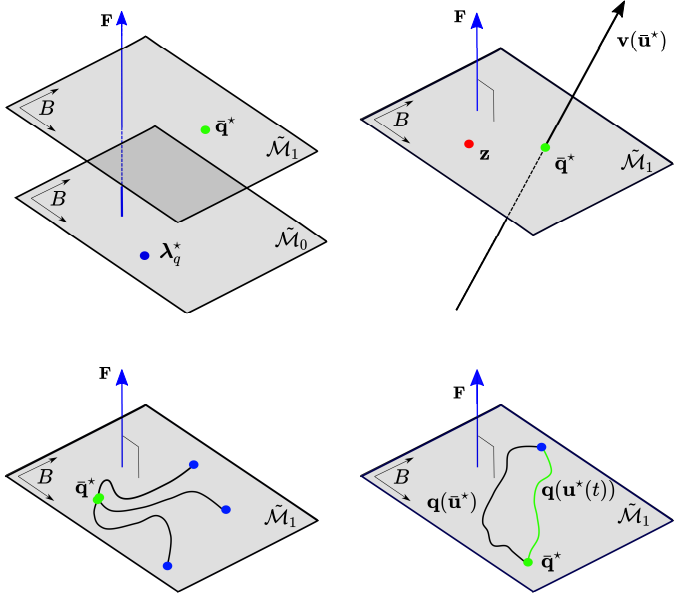


Figure 1. Illustration of the main properties of the FEM discretization. *Top left*: Duality between state and adjoint when the adjoint is solved with a zero-mean constraint. *Top right*: Interpretation of the state problem as an eigenvector optimization problem for the kernel of the state operator, which is spanned by $\mathbf{v}(\mathbf{u})$. *Bottom left*: From any initial condition in $\tilde{\mathcal{M}}_1$, the state asymptotically converges to \bar{q}^* while remaining in $\tilde{\mathcal{M}}_1$. *Bottom right*: Dynamic optimization procedure exploiting knowledge of the initial condition and of the static optimal solution.

the control field varies smoothly over the domain and does not have steep gradients. We simulated the system under the constant control field $\bar{\mathbf{u}}^*$ for three different initial densities. Figure 3 shows that for each initial condition, $\bar{\mathbf{u}}^*$ stabilizes the discretized state \mathbf{q} to the corresponding optimal equilibrium density \bar{q}^* . We then solve the modified dynamic problem to optimize the convergence rate to equilibrium from the initial condition $\mathbf{q}_0^{(1)}$, which is defined as a Gaussian density centered at $(-0.5, -0.5)$. Convergence of the solutions of both the static and dynamic problems to the optimal solution is evidenced by the plots of the cost functional J and $\|\nabla J\|$ in Figure 4. Figure 5 shows that the time-varying control field $\mathbf{u}^*(t)$ produces faster convergence to the optimal equilibrium density than $\bar{\mathbf{u}}^*$ and that $\mathbf{u}^*(t) \rightarrow \bar{\mathbf{u}}^*$ for sufficiently large T . Finally, Figures 6 and 7 plot several snapshots of the density evolution under both control fields, $\bar{\mathbf{u}}^*$ and $\mathbf{u}^*(t)$. Figure 7 shows that $\mathbf{u}^*(t)$ at $t = 0$ [s] exhibits its highest magnitude near the peak of the initial density; this concentration of control effort enables it to drive the swarm around the obstacle to the target equilibrium density faster than $\bar{\mathbf{u}}^*$.

In test case 2, we fabricate a somewhat pathological case in which the target density has non-compact support and the domain is partially bisected by a rectangular obstacle. The optimal control field from the static OCP generates a unique equilibrium, as proven in Theorem 3, but the density may be very slow to converge to this equilibrium, depending on the initial condition. Figure 8 plots the target density z , the solution \bar{q}^* , $\bar{\mathbf{u}}^*$ of the static optimization problem, and the norm of $\bar{\mathbf{u}}^*$. As in test case 1, \bar{q}^* is smooth, non-negative, and close to z , and $\bar{\mathbf{u}}^*$ varies smoothly over Ω and lacks

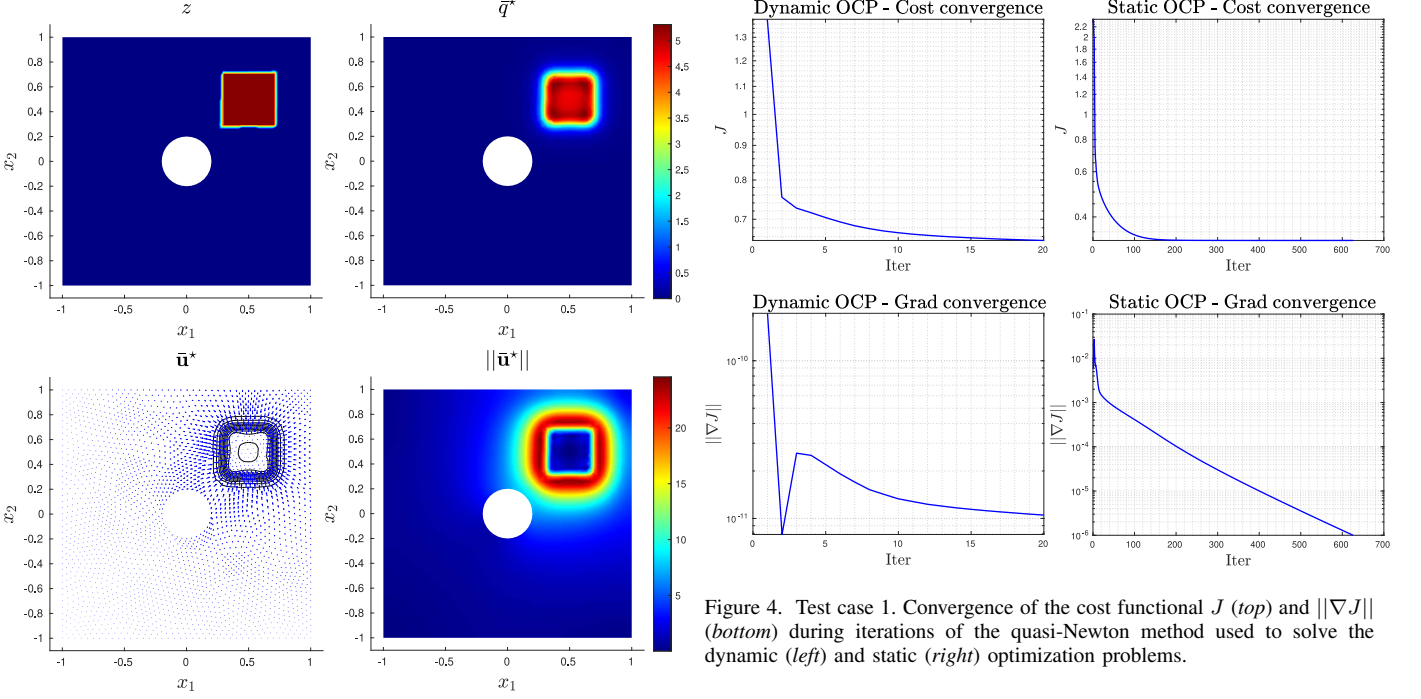


Figure 2. Test case 1. Equilibrium density \bar{q}^* and control field \bar{u}^* computed from the static optimization problem, in which z is a non-smooth target function. The control weights are $\alpha = 1$, $\beta = 10^{-3}$, and $\beta_g = 10^{-5}$.

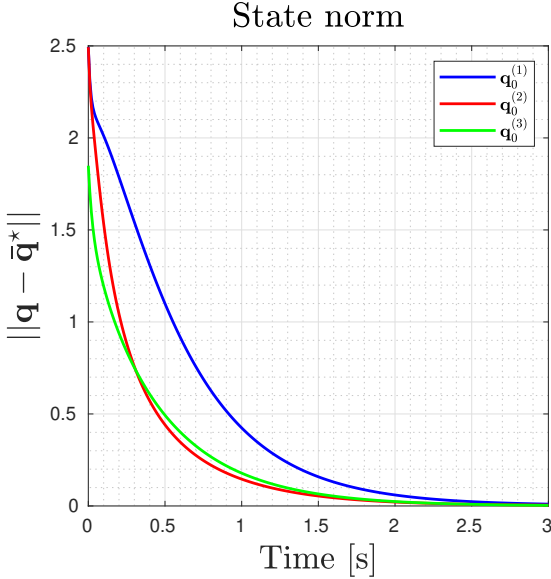


Figure 3. Test case 1. Convergence in the L^2 norm to the optimal equilibrium \bar{q}^* from three different initial conditions, $q_0^{(1)}$, $q_0^{(2)}$, and $q_0^{(3)}$, where $q_0^{(1)}$ and $q_0^{(2)}$ are Gaussian densities centered at $(-0.5, -0.5)$ and $(-0.5, 0.5)$, respectively, and $q_0^{(3)}$ is the uniform density over the domain Ω .

steep gradients. We solved the dynamic problem to optimize the convergence rate of the density to \bar{q}^* from an initial distribution that is located on the left side of the obstacle, closer to the left peak of z (Fig. 9, top row). Figure 9 presents several snapshots of the density evolution under both the constant and time-varying control fields, \bar{u}^* and $u^*(t)$. The figure shows that within the first 0.6 [s], the constant field \bar{u}^*

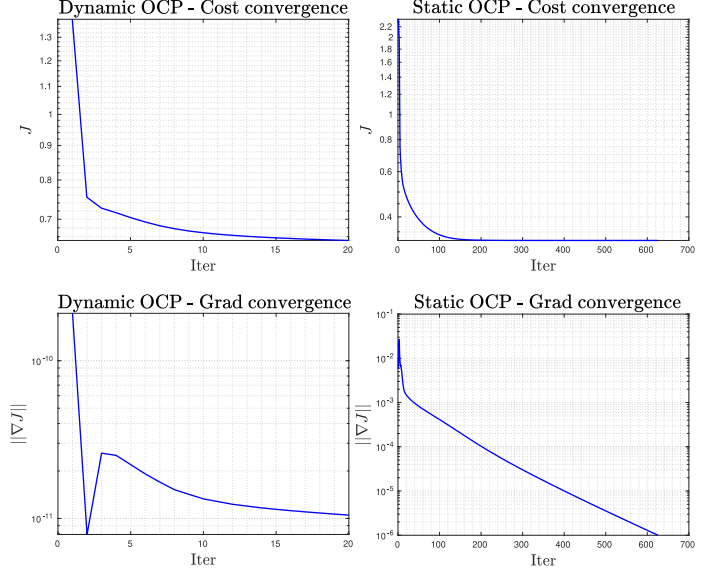


Figure 4. Test case 1. Convergence of the cost functional J (top) and $\|\nabla J\|$ (bottom) during iterations of the quasi-Newton method used to solve the dynamic (left) and static (right) optimization problems.

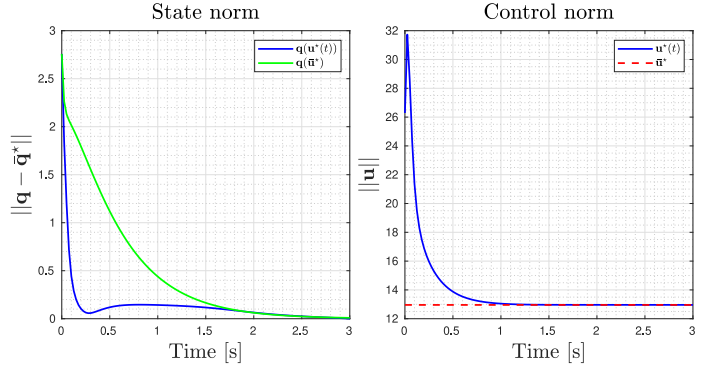


Figure 5. Test case 1. Convergence in the L^2 norm of the solution of the dynamic optimization problem to its static counterpart. Left: Norm convergence of the density q to the optimal equilibrium \bar{q}^* under the constant control field \bar{u}^* (green) and the time-varying control field $u^*(t)$ (blue). Right: Norm convergence of $u^*(t)$ to \bar{u}^* .

drives the density mostly toward the left peak of z , whereas the time-varying field $u^*(t)$ splits the density between the two peaks. Figure 10 indicates that due to this splitting, $u^*(t)$ produces faster convergence to the optimal equilibrium density than \bar{u}^* by two orders of magnitude; the density under \bar{u}^* eventually converges to the equilibrium by around 100 [s].

In test case 3, we consider a scenario with an external velocity field $\mathbf{b} \in L^\infty(\Omega)^2$ and a more complex domain Ω with multiple obstacles. Introducing the drift velocity field \mathbf{b} into the weak formulation of the state equation in the static OCP, we obtain the following problem: find $q \in \mathcal{M}_1$ such that

$$\int_{\Omega} \left(\mu \nabla q \cdot \nabla v - (\mathbf{u} + \mathbf{b}) q \nabla v \right) d\Omega = 0 \quad \forall v \in H^1(\Omega).$$

The discretization of this state equation is:

$$(A - \mathbb{B}^\top \mathbf{u} - B^\top) \mathbf{q} = \mathbf{0},$$

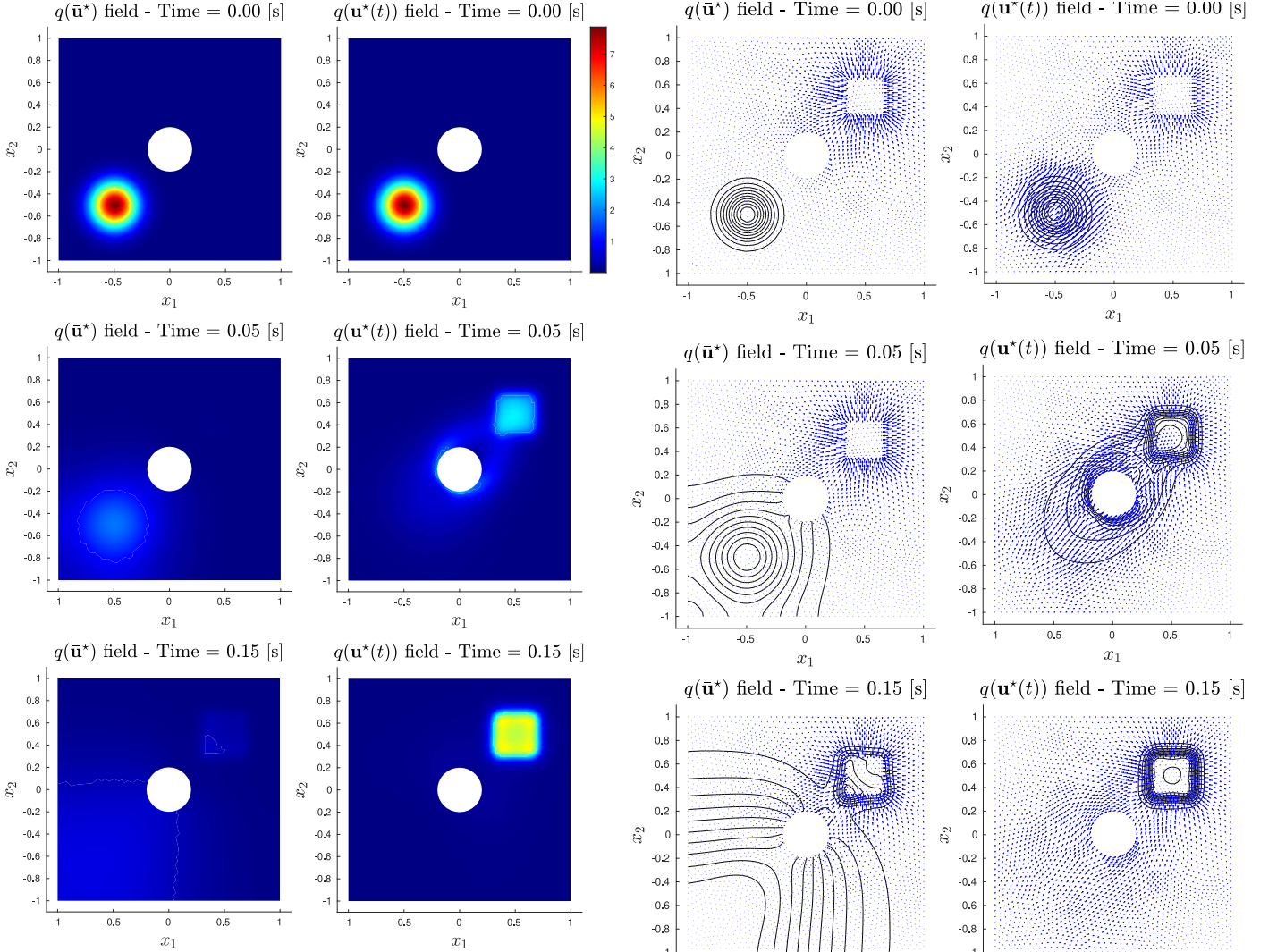


Figure 6. Test case 1. Density evolution under (left) the optimal constant control field $\bar{\mathbf{u}}^*$, and (right) the optimal time-varying control field $\mathbf{u}^*(t)$, which is optimized for the initial condition but converges to $\bar{\mathbf{u}}^*$ over time.

where B is the transport matrix associated with \mathbf{b} , defined as $B_{ij} = \int_{\Omega} \mathbf{b} \cdot \nabla \phi_i \phi_j d\Omega$. The state equation in the dynamic OCP is modified in a similar way. Note that the additional advection term does not affect the results that we have previously derived for the OCPs. Figure 11 plots the target density z , the solution \bar{q}^* , $\bar{\mathbf{u}}^*$ of the static optimization problem, and the norm of $\bar{\mathbf{u}}^*$, which exhibit similar properties to the corresponding plots for the other two test cases. The drift field \mathbf{b} is defined as $\mathbf{b} = [-\sin(\pi x_1) \cos(\pi x_2); \cos(\pi x_1) \sin(\pi x_2)]$. We solved the dynamic problem to obtain the time-varying control field $\mathbf{u}^*(t)$ that optimizes the convergence rate of the density to \bar{q}^* from an initial condition defined as the indicator function of a square that is located at the bottom-left of the domain. Figure 12 compares the convergence rate of the density to the corresponding equilibrium under \mathbf{b} alone (uncontrolled), $\mathbf{b} + \bar{\mathbf{u}}^*$, and $\mathbf{b} + \mathbf{u}^*(t)$, and Figure 13 plots several snapshots of the density evolution under $\mathbf{b} + \bar{\mathbf{u}}^*$ and $\mathbf{b} + \mathbf{u}^*(t)$. The uncontrolled density converges to the equilibrium induced by the drift field \mathbf{b} . The constant control $\bar{\mathbf{u}}^*$ stabilizes the optimal

Figure 7. Test case 1. Evolution of density contours (black) under the optimal control fields (blue), $\bar{\mathbf{u}}^*$ (left) and $\mathbf{u}^*(t)$ (right).

equilibrium density \bar{q}^* in the presence of the drift field, while the time-varying control $\mathbf{u}^*(t)$ speeds up the convergence to this equilibrium.

V. CONCLUSIONS

In this paper, we have proposed a density control strategy for swarms of robots that follow single-integrator advection-diffusion dynamics. We formulated and solved an Optimal Control Problem (OCP) based on the mean-field model of the swarm to compute a space-dependent control field, defined as the robots' velocity field, that does not require inter-robot communication or density estimation algorithms for implementation. We proved that the equilibrium density of the controlled system is globally asymptotically stable, thus demonstrating that the optimal control law is robust to transient perturbations and independent of the initial conditions. For cases where the initial condition is approximately known, a modified dynamic OCP was formulated to speed up con-

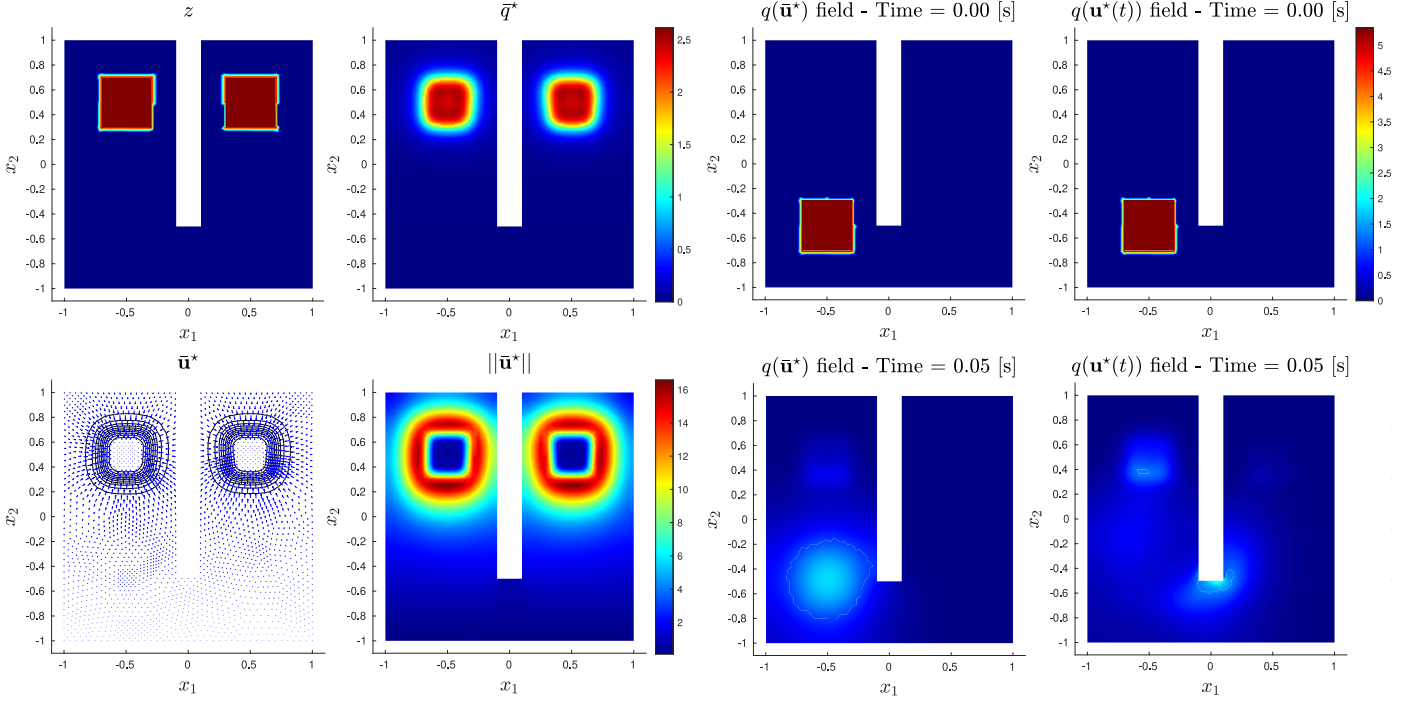


Figure 8. Test case 2. Equilibrium density \bar{q}^* and control field \bar{u}^* computed from the static optimization problem, in which z is a non-smooth target function composed of the disjoint union of two characteristic functions. The peaks of z are separated by an obstacle, which prevents density transport directly between the peaks. The control weights are $\alpha = 1$, $\beta = 10^{-3}$, and $\beta_g = 10^{-5}$.

vergence to the optimal equilibrium density. Thanks to the turnpike property, the optimal solution of the dynamic OCP converges to its static counterpart, thus ensuring the stability and robustness of the control law computed by this OCP. The analysis of the static and dynamic OCPs has been consistently carried out for both their infinite-dimensional formulations and their finite-dimensional discretizations. This analysis shows that several useful properties of the OCPs are inherited by the FEM discretizations.

Future work includes two main research directions. From a theoretical standpoint, we can extend our density control approach to swarms with explicit interactions between robots. This problem is addressed in [32] using methods from multimarginal optimal transport, whereas our approach would entail the formulation of a static OCP that is subject to an advection-diffusion PDE with nonlocal components in the advection field and is amenable to the stability and robustness analyses presented in this paper. We can also test the effectiveness of the control law in practice by implementing it on real robots, which will require incorporating real-world motion constraints.

REFERENCES

- [1] M. Dorigo, G. Theraulaz, and V. Trianni, “Swarm Robotics: Past, Present, and Future,” *Proceedings of the IEEE*, vol. 109, no. 7, pp. 1152–1165, 2021.
- [2] K. Elamvazhuthi and S. Berman, “Mean-field models in swarm robotics: A survey,” *Bioinspiration and Biomimetics*, vol. 15, no. 1, 2019.
- [3] M. A. Hsieh, A. Halász, S. Berman, and V. Kumar, “Biologically inspired redistribution of a swarm of robots among multiple sites,” *Swarm Intelligence*, vol. 2, no. 2, pp. 121–141, 2008.

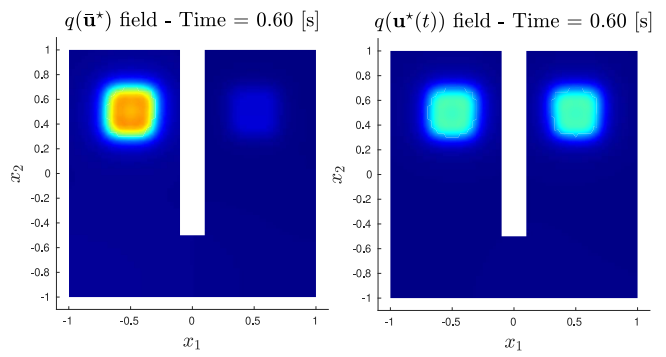


Figure 9. Test case 2. Density evolution under (left) the optimal constant control field \bar{u}^* , and (right) the optimal time-varying control field $u^*(t)$, which is optimized for the initial condition but converges to \bar{u}^* over time.

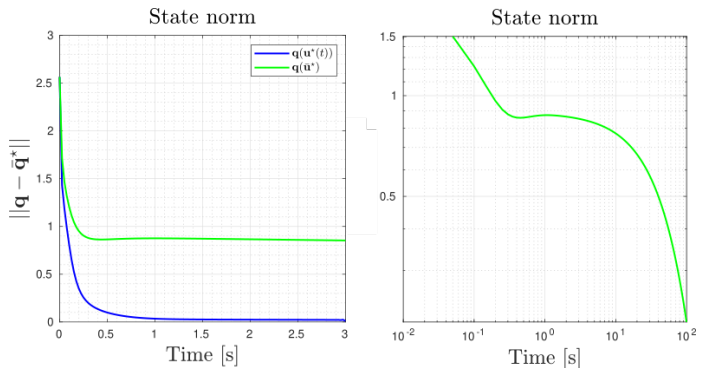


Figure 10. Test case 2. Convergence in the L^2 norm of the density q to the optimal equilibrium \bar{q}^* under the constant control field \bar{u}^* (green) and the time-varying control field $u^*(t)$ (blue), over (left) the first 3 [s]; (right) 100 [s] (\bar{u}^* only, log-log scale).

- [4] K. Elamvazhuthi, H. Kuiper, and S. Berman, “PDE-based optimization for stochastic mapping and coverage strategies using robotic ensembles,” *Automatica*, vol. 95, pp. 356–367, 2018.
- [5] V. Krishnan and S. Martínez, “A multiscale analysis of multi-agent

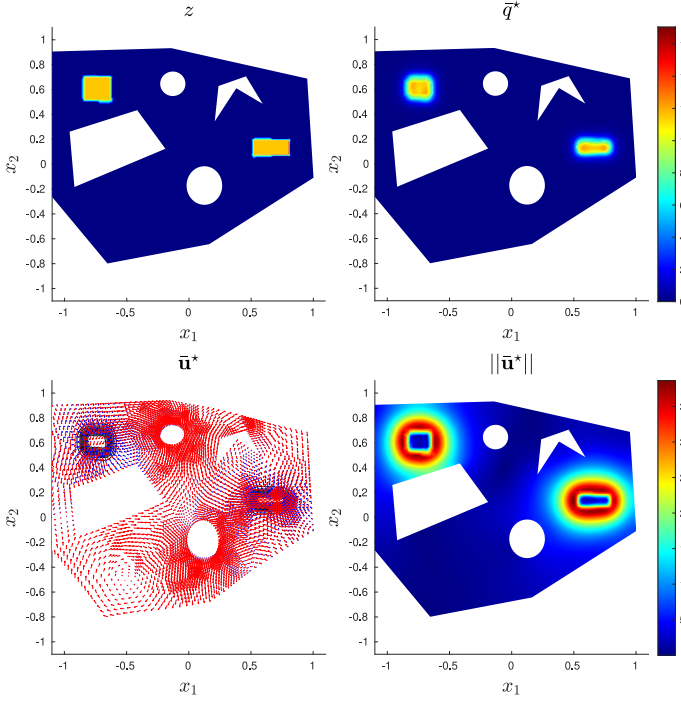


Figure 11. Test case 3. Equilibrium density \bar{q}^* and control field \bar{u}^* computed from the static optimization problem, in which z is a non-smooth target function composed of the disjoint union of two characteristic functions. The drift vector field \mathbf{b} is shown in red in the bottom-left plot, in addition to the control vector field \bar{u}^* in blue. The control weights are $\alpha = 1$, $\beta = 10^{-3}$, and $\beta_g = 10^{-5}$.

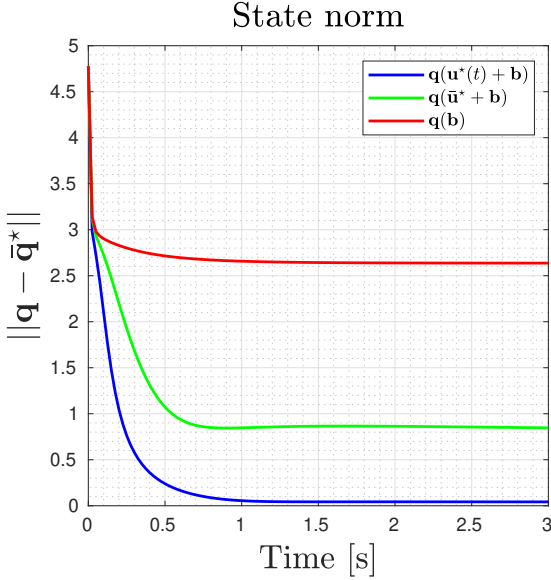


Figure 12. Test case 3. L^2 -distance between the optimal equilibrium density \bar{q}^* and the density q under the sum of the drift velocity field \mathbf{b} and (red) no control velocity field; (green) the optimal constant control field \bar{u}^* ; and (blue) the optimal time-varying control field $u^*(t)$.

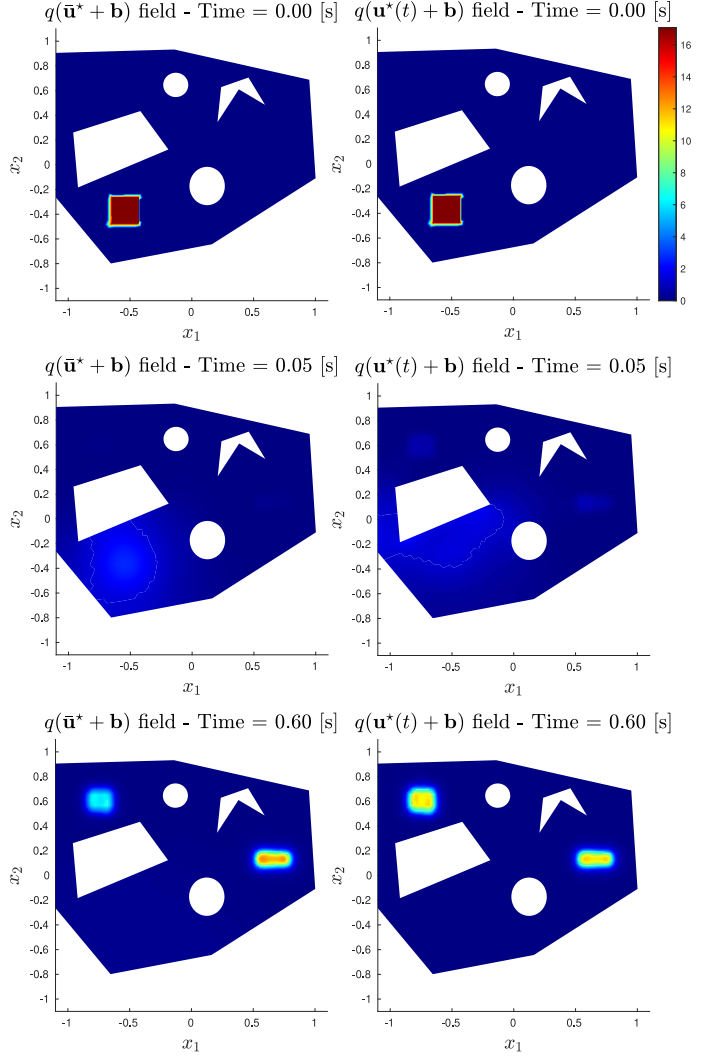


Figure 13. Test case 3. Density evolution under the joint effect of the drift vector field \mathbf{b} and (left) the optimal constant control \bar{u}^* , or (right) the optimal time-varying control field $u^*(t)$, which is optimized for the initial condition but converges to \bar{u}^* over time.

- [8] U. Eren and B. Aćikmeşe, “Velocity field generation for density control of swarms using heat equation and smoothing kernels,” *IFAC-PapersOnLine*, vol. 50, no. 1, pp. 9405–9411, 2017.
- [9] B. Aćikmeşe and D. S. Bayard, “A Markov chain approach to probabilistic swarm guidance,” in *2012 American Control Conference (ACC)*. IEEE, 2012, pp. 6300–6307.
- [10] S. Roy, M. Annunziato, A. Borzì, and C. Klingenberg, “A Fokker–Planck approach to control collective motion,” *Computational Optimization and Applications*, vol. 69, no. 2, pp. 423–459, 2018.
- [11] C. Sinigaglia, A. Manzoni, and F. Braghin, “Density control of large-scale particles swarm through PDE-constrained optimization,” *arXiv preprint arXiv:2104.06373*, 2021.
- [12] K. Elamvazuthi, H. Kuiper, M. Kawski, and S. Berman, “Bilinear controllability of a class of advection–diffusion–reaction systems,” *IEEE Transactions on Automatic Control*, vol. 64, no. 6, pp. 2282–2297, 2019.
- [13] T. Zheng, Q. Han, and H. Lin, “Transporting robotic swarms via mean-field feedback control,” *IEEE Transactions on Automatic Control*, 2021.
- [14] ———, “Distributed mean-field density estimation for large-scale systems,” *IEEE Transactions on Automatic Control*, 2021.
- [15] J.-D. Benamou and Y. Brenier, “A computational fluid mechanics solution to the Monge–Kantorovich mass transfer problem,” *Numerische Mathematik*, vol. 84, no. 3, pp. 375–393, 2000.
- [16] J. Droniou and J.-L. Vázquez, “Noncoercive convection–diffusion elliptic problems with Neumann boundary conditions,” *Calculus of Variations and Partial Differential Equations*, vol. 57, no. 1, p. 14, 2018.

coverage control algorithms,” *arXiv preprint arXiv:2102.11411*, 2021.

- [6] S. Berman, A. Halász, M. A. Hsieh, and V. Kumar, “Optimized stochastic policies for task allocation in swarms of robots,” *IEEE Transactions on Robotics*, vol. 25, no. 4, pp. 927–937, 2009.
- [7] S. Bandyopadhyay, S.-J. Chung, and F. Y. Hadaegh, “Probabilistic and distributed control of a large-scale swarm of autonomous agents,” *IEEE Transactions on Robotics*, vol. 33, no. 5, pp. 1103–1123, 2017.

tions and Partial Differential Equations, vol. 34, no. 4, pp. 413–434, 2009.

[17] S. Salsa, *Partial differential equations in action: from modelling to theory*. Springer, 2016.

[18] A. Manzoni, S. Salsa, and A. Quarteroni, *Optimal Control of Partial Differential Equations, Analysis, Approximation and Applications*. Springer, 2021.

[19] E. Trélat and E. Zuazua, “The turnpike property in finite-dimensional nonlinear optimal control,” *Journal of Differential Equations*, vol. 258, no. 1, pp. 81–114, 2015.

[20] E. Trélat, C. Zhang, and E. Zuazua, “Steady-state and periodic exponential turnpike property for optimal control problems in Hilbert spaces,” *SIAM Journal on Control and Optimization*, vol. 56, no. 2, pp. 1222–1252, 2018.

[21] P. Bochev and R. B. Lehoucq, “On the finite element solution of the pure Neumann problem,” *SIAM Review*, vol. 47, no. 1, pp. 50–66, 2005.

[22] A. Quarteroni, *Numerical Models for Differential Problems*. Springer Publishing Company, 2016.

[23] C. Bolley and M. Crouzeix, “Conservation de la positivité lors de la discréétisation des problèmes d’évolution paraboliques,” *RAIRO. Analyse Numérique*, vol. 12, no. 3, pp. 237–245, 1978.

[24] J. Xu and L. Zikatanov, “A monotone finite element scheme for convection-diffusion equations,” *Mathematics of Computation*, vol. 68, no. 228, pp. 1429–1446, 1999.

[25] V. Thomée, “On positivity preservation in some finite element methods for the heat equation,” in *International Conference on Numerical Methods and Applications*. Springer, 2014, pp. 13–24.

[26] Y. Zhang, X. Zhang, and C.-W. Shu, “Maximum-principle-satisfying second order discontinuous Galerkin schemes for convection-diffusion equations on triangular meshes,” *Journal of Computational Physics*, vol. 234, pp. 295–316, 2013.

[27] V. Thomée and L. Wahlbin, “On the existence of maximum principles in parabolic finite element equations,” *Mathematics of Computation*, vol. 77, no. 261, pp. 11–19, 2008.

[28] M. S. Aronna and F. Tröltzsch, “First and second order optimality conditions for the control of Fokker-Planck equations,” *ESAIM: Control, Optimisation and Calculus of Variations*, vol. 27, p. 15, 2021.

[29] R. Glowinski, Y. Song, X. Yuan, and H. Yue, “Bilinear optimal control of an advection-reaction-diffusion system,” *SIAM Review*, vol. 64, no. 2, pp. 392–421, 2022.

[30] A. Quarteroni, A. Manzoni, and F. Negri, *Reduced Basis Methods for Partial Differential Equations: An Introduction*. Springer International Publishing, 2015.

[31] B. W. Bader and T. G. Kolda, “Algorithm 862: MATLAB tensor classes for fast algorithm prototyping,” *ACM Transactions on Mathematical Software*, vol. 32, no. 4, p. 635–653, Dec. 2006.

[32] Y. Chen, “Density control of interacting agent systems,” *arXiv preprint arXiv:2108.07342*, 2021.



Andrea Manzoni Andrea Manzoni received the M.Sc. Degree in Mathematical Engineering from Politecnico di Milano, Italy, in 2008, and the Ph.D. in Mathematics from the Ecole Polytechnique Fédérale de Lausanne (EPFL), Switzerland, in 2012. He has been research fellow at the International School of Advanced Studies, Trieste, Italy, until 2014, and researcher at EPFL until 2017, when he became tenure-track Assistant Professor at Politecnico di Milano. Since 2020 he is Associate Professor of Numerical Analysis at Politecnico di Milano.



Francesco Braghin Francesco Braghin received the M.Sc. degree in mechanical engineering and the Ph.D. degree in applied mechanics both from Politecnico di Milano, Italy, in 1997 and 2001, respectively. He became a Researcher, in 2001 and in 2011 an Associate Professor in the Department of Mechanical Engineering, Politecnico di Milano, where, since 2015, he has been a Full Professor in applied mechanics.



Spring Berman received the M.S.E. and Ph.D. degrees in Mechanical Engineering and Applied Mechanics from the University of Pennsylvania in 2008 and 2010, respectively. From 2010 to 2012, she was a Postdoctoral Fellow in Computer Science at Harvard University. She was then an Assistant Professor of Mechanical and Aerospace Engineering at Arizona State University, where she has been an Associate Professor since 2018. Her research focuses on the analysis of behaviors in biological and engineered collectives and the synthesis of control strategies for robotic swarms.



Carlo Sinigaglia Carlo Sinigaglia is a Ph.D. Candidate in Mechanical Engineering at Politecnico di Milano. He obtained the M.Sc. in Mechanical Engineering from Politecnico di Milano, Italy, in 2019. His research interests include swarm robotics, macroscopic modeling of large-scale dynamical systems and optimal control.